Characterization of thermally annealed PEEK and CFR-PEEK composites: Structure-properties relationships

Accepted Manuscript

Characterization of thermally annealed PEEK and CFR-PEEK composites: Structure-properties relationships

Marco Regis, Anuj Bellare, Tommaso Pascolini, Pierangiola Bracco

PII: S0141-3910(16)30383-4

DOI: 10.1016/j.polymdegradstab.2016.12.005

Reference: PDST 8126

To appear in: *Polymer Degradation and Stability*

Received Date: 14 July 2016

Revised Date: 24 November 2016

Accepted Date: 15 December 2016

Please cite this article as: Regis M, Bellare A, Pascolini T, Bracco P, Characterization of thermally annealed PEEK and CFR-PEEK composites: Structure-properties relationships, *Polymer Degradation and Stability* (2017), doi: 10.1016/j.polymdegradstab.2016.12.005.

Characterization of thermally annealed PEEK and CFR-PEEK composites: structure-properties relationships

Marco Regis[1, 2], Anuj Bellare[3], Tommaso Pascolini[2], Pierangiola Bracco[1*]

[1] Department of Chemistry and NIS Center, University of Turin, Turin, Italy

[2] R&D Department, Limacorporate SpA

[3] Department of Orthopedic Surgery, Brigham and Women's Hospital, Harvard Medical School, Boston, MA 02115, USA

* Corresponding author:
Pierangiola Bracco
Department of Chemistry and NIS Center,
University of Turin,
Via Pietro Giuria, 7
10125 Torino, ITALY
Phone: +39 011 6707547
Fax: +39 011 6707855
e-mail: pierangiola.bracco@unito.it

Abstract

The structure-properties correlation of neat and carbon fiber reinforced (CFR) PEEK, subjected to thermal annealing, was investigated. The polymer and its composites (30% w/w carbon fibers, PAN or pitch based) underwent annealing treatments at 200, 225, 250, 275 and 300°C. The resulting morphology was investigated by Differential Scanning Calorimetry (DSC), Fourier Transform InfraRed (FTIR) spectroscopy, Wide Angle X-ray Diffraction (WAXD) and Small Angle X-ray Scattering (SAXS), while the flexural peak load from a bending test and the reduced elastic modulus from nanoindentation measurements were chosen as markers of the mechanical properties. The morphological investigation showed that annealing induces an increase in crystallinity, by a combination of thickening of the existing lamellae and nucleation and growth of new, thinner lamellae. Although the mechanical properties showed highly significant differences depending upon the reinforcement type, we were able to induce a significant increase (form 9 to 12%) in the flexural peak load with the annealing treatments, regardless of the material formulation. The reduced elastic

modulus of all PEEK and CFR PEEK formulations also increased with increasing the annealing temperature.

In summary, this investigation provides an evidence of how appropriate thermal treatments can be used to tune the mechanical properties of both PEEK and CFR PEEK.

Keywords: PEEK, carbon fiber, crystallization, annealing.

1. Introduction

Poly(etheretherketone) (PEEK) is a high-temperature resistant semicrystalline polymer, possessing excellent mechanical properties and chemical inertness. To date, PEEK has been studied as a high performance polymer in a wide variety of applications, from high temperature bearings to aerospace, including as a biomaterials for dental or orthopedic applications, due to its excellent wear resistance and strength-to-weight ratio [1–3].

As for every semi-crystalline polymer, the macroscopic mechanical properties of PEEK largely depend on the morphology induced by the processing conditions [4]. The crystalline unit cell, lamellar and spherulitic structure of PEEK have been extensively investigated over the years [5–7]. Literature findings indicate that PEEK chains in the lamellar regions form an orthorhombic crystal structure. Based on X-ray diffraction studies, the c-axis of the orthorhombic unit cell of PEEK spans three aryl groups, with a center-to-center distance between aryl groups of 5Å, corresponding to a long-axis length of 15Å [8]. Like most semicrystalline polymers of medium molecular weight, the macromolecules of PEEK fold into fine lamellae radiating out from a nucleus to form 5-10 μm size spherulites [9]. The thickness of lamellae, as well as the size and density of spherulites, depends on the thermal history [4,10–12]. This observation has stimulated extensive research on how crystallization conditions affect crystal morphology and properties of PEEK and its composites [13–17]. In particular, there have been several investigations in which the degree of crystallinity was measured at various heating rates using differential scanning calorimeters (DSC), showing that crystallization in PEEK is much more complex than that of other thermoplastic polymers [18,19]. In addition, multi-peak endotherms were observed, as have been observed for other thermoplastic polymers [20–22]. Several interpretations have been proposed to explain the origin of this double melting behavior: among other, a dual lamellar thickness model [13,23], simultaneous melting and re-crystallization [3,24] or physical ageing [25]. Although the phenomenon has been discussed in detail, there is still debate on its interpretation [26–28].

The mechanical properties of PEEK have also been extensively studied. A large body of literature is present on the mechanical properties of PEEK and carbon fiber-reinforced (CFR) PEEK and their stability over a range of working conditions, such as aqueous or high temperature environment [29–31]. Nonetheless, these studies provide poor or no data that relate the polymer morphology and physical properties. Furthermore, the differences in thermal treatments, heating rates and calculation formulas among these previous studies preclude the development of a correlation between the crystallographic morphology and macroscopic properties of unfilled and CFR-PEEK [6].

In recent years, reinforced composites prepared by adding glass or carbon fibers to the PEEK matrix have been studied and evaluated for various applications [2,32–36]. The type and content of fibers, their length and orientation, as well as the nature of the polymeric matrix and the fiber-matrix interface are considered to be the variables determining the mechanical behavior of such composites [15]. Macro and micro-mechanical models that take into account all these morphological parameters have been proposed, and are used in the design of reinforced polymer composites [37]. However, it has been demonstrated that also the crystallinity of the polymer matrix has an impact on the properties of the resulting composite, for polymer matrixes such as polyamides, poly(ethylene terephthalate), poly(phenylene suphide) and PEEK [38], with the formation of crystal nuclei at the fiber-matrix interface in a process known as trans-crystallization. The crystallization of PEEK in the presence of fibers has been the subject of investigations focused mainly on the effect of fiber addition to the matrix crystallinity and crystallization behavior [39,40] and the effect of fiber on fracture mechanics [30]. However, these structure-property relationships still need to be fully understood. Moreover, to date, systematic studies correlating PEEK crystallinity, fiber characteristics, and mechanical properties have not yet been sufficiently developed.

This work aims therefore to provide more information on such structure-property relationships through a comprehensive study conducted by:

- Differentiating PEEK and CFR PEEK crystallinity using annealing treatments
- Assessing the extent of crystal structure modification through Differential Scanning Calorimetry (DSC), Fourier Transform Infra-Red spectroscopy (FT-IR), and X-ray (Wide Angle X-ray diffraction, WAXD; and Small Angle X-ray Scattering, SAXS) techniques, in order to obtain reliable and univocal information on PEEK and CFR PEEK melting behavior, and to provide at the same time additional details on lamellar thicknesses, dimensions, and crystal morphology in the differentiated crystal structures
- Providing PEEK and CFR PEEK mechanical characterization by testing the annealed samples for static mechanical properties (bending) and hardness as a function of the resulted differentiated crystallinity.

2. Materials and methods

Materials were supplied as granules by Invibio (Invibio Ltd, Lancashire, UK). Materials trade names were Ni1, Ni1CA30 and Motis- an unfilled PEEK, a 30% wt. PAN carbon fiber and a 30% wt. pitch carbon fiber reinforced PEEK composite, respectively. For better clarity, materials will be referred hereafter as U, O, and M, indicating Ni1, Ni1CA30 and Motis, respectively. Given the

differences in chemical nature and structure (PAN fibers are derived from the polyacrylonitrile graphitization, and thus have much more aligned domains along the principal fiber axis in respect to pitch fibers, that in turn come from the processing of bituminous substances and thus have a less oriented graphitic structure) the two different carbon fibers types had different mechanical properties and dimensions: Young's modulus and fiber diameter were 540 GPa and 6±2 μm for PAN carbon fibers and 280 GPa and 10±2μm for pitch carbon fibers, respectively. In previous studies, the different nature of the two carbon fibers has shown to give different material properties in terms of mechanical strength and modules, as well as in the crystallization behavior of the tested materials [40,41].

Sample preparation consisted of various steps: granules were preheated to 70°C to remove the residual moisture, and then injection molded into 127x12.7x3.7 mm specimens. Nozzle temperature was maintained at 400°C, higher than the PEEK matrix melting temperature T_m (343°C), to facilitate material flow in the mold, which was maintained at 250°C. Polymer flow and holding time took 2.5 minutes, in order to allow the polymer to fill the mold volume, then the mold was opened and specimens were naturally cooled in air, which reached room temperature in approximately 5 to 6 minutes. Considering that polymer injection takes place in a very short time, it is possible to state therefore that the material underwent a temperature gradient from 400°C to RT within an overall time range of about 3 to 9 minutes. Since the samples were completely cooled down after the above mentioned steps, and taking into account that the thermal conductivity of the material is low, it is believed that the overall thermal history imparted to the polymer with the injection molding procedure (that is, the overall sample cooling conditions) corresponds to a non-linear cooling rate included in the 40°C/min-125°C/min span.

The crystallinity of the three PEEK injection molded samples formulations was then differentiated by annealing treatments. The chosen annealing temperatures were 200, 225, 250, 275, and 300°C, respectively. Specimens were heated up at a constant rate of 5°C/min in a programmable B180 oven (Nabertherm, D), held at the chosen temperature for 5h, and then air cooled to 20°C. Figure 1 reports the performed thermal treatments.

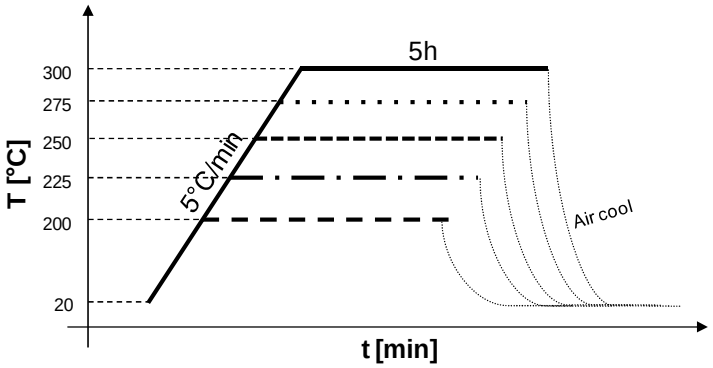

Figure 1. Temperature versus time variation in annealing treatments performed on Ni1, Motis, and Ni1CA30.

A Q20 differential scanning calorimeter (TA Instruments, New Castle, DE, USA) was used to assess the polymer crystallinity. 6.5 to 8.5 mg samples were prepared from the injection molded samples, by cutting a portion of the specimen at the corner edge throughout the entire specimen thickness. Samples were then encapsulated into hermetic pans and subjected to DSC scans. DSC apparatus was calibrated with Indium and all tests were run in triplicate. The samples were heated up to 400°C at 20°C/min. The scan rate of 20°C/min was chosen as a compromise to minimize recrystallization on heating and to maintain enough accuracy [42]. % Crystallinity was calculated according to (1)

$$X\% = \frac{\text{melting peak area}}{130} / v_m \cdot 100 \quad (1)$$

where v_m is the fiber content, when applicable [43] and 130J/g is the theoretical heat of fusion of pure crystalline PEEK [5].

Peak area was calculated with integration algorithms in TA Universal Analysis 2000 SW (TA inc, USA), using the 200-400°C interval for each of the collected thermograms. According to the slope of the curve, sigmoidal tangential interpolation was used. Double peaks were separately processed in all samples except for 300°C annealed samples, where consistent peak overlapping was observed. In the latter case, a single integration step was applied for both signals.

Fourier Transform Infrared Spectroscopy (FTIR) was performed in specular reflectance mode using a Perkin Elmer Spotlight 300 microscope (Perkin Elmer, US). All spectra were collected on a 100x100μm spot size on the samples surface, with 16 scans at a 4cm^{-1} resolution in the 700-4000cm^{-1} region. Crystallinity was evaluated by transforming the reflectance spectra with the

Kramers-Kronig algorithm into absorption index spectra, and then by evaluating the 1305/1280cm^{-1} band ratio [44].

Wide angle X-ray diffraction (WAXD) measurements on the injection molded and annealed specimens were collected using a Rigaku S-Max 300 instrument operating with CuKα X-rays of wavelength 1.54Å. The X-ray point source was generated by a rotating anode operating at 40kV and 30mA. Injection molded specimens were cut into sections, approximately 1mm thick, in order to be positioned in the sample holder. Sectioning was performed with a diamond blade mounted on an automated Mecatome T330 metallographic cutting machine (Presi, F). Scans were performed with a 2θ amplitude of 0.09° < 2θ < 41.63°. Data were recorded as signal counts for each of the scanned 2θ angle.

The same Rigaku S-Max 300 CuKα rotating anode instrument was used to obtain Small Angle X-ray Scattering (SAXS) data, with an X-ray source operating at 40kV and 30mA. The beam had a pinhole collimation which resulted in a beam diameter of approximately 0.3mm. Scattered X-rays travelled through an evacuated tube to reduce background scattering and to increase the signal/noise ratio. Data were recorded as scattering intensity I (counts) as a function of the scattering vector q expressed as

$$q = \left(\frac{4\pi}{\lambda}\right)\sin\theta \tag{3}$$

Where λ is the X-rays wavelength and θ is half of the scattering angle 2θ. Scattering intensity was collected by a Pilatus 300k pixel-detector at a distance of approximately 1500mm from the sample, with an angular scattering ranging from q=6.49x10^{-3} nm^{-1} to q=2.79 nm^{-1}. Radially averaged scattering curves were normalized and subtracted by their respective background curve taking into account the thermal diffusive scattering contribution following Porod's extrapolation.

Specimens were also tested in order to assess their static mechanical properties. A 3-point static bending test was then performed, in order to investigate the resulting flexural properties of all the samples considered. A MTS mini Bionix II 858 universal machine (MTS, US), equipped with a 15kN class 0.5-certified load cell was used. Tests were conducted at a crosshead speed of 5mm/min until specimens failure or breakage, according to ASTM D790 [45].

Micro-hardness test was performed using a Fischerscope HM2000 micro indenter (Fischer, D) equipped with a 4x4µm (principal direction) Vickers tip. The samples were cut into sections and polished up to 0.05-0.1µm roughness prior to the test. The experiment was conducted in continuous indentation mode at a constant loading/unloading rate of 300µN/sec to a maximum depth of 5000nm. Load holding segments, 20s at maximum load for material creep and 50s after 80% unloading or until 0.4µN load, whichever occurred first (for thermal drift corrections) were also implemented [46]. Each sample was indented at 15 different positions at least 100µm apart. Particular attention was put in examining the bulk region as well as the fiber-matrix interface, by indenting the polymer matrix in the non-reinforced areas and in the adjacent region of the matrix-fiber interface. For the latter, only circular fiber sections were selected (vertically oriented fibers), so as not to impact the tip with underlying fiber sections. This approach has been extensively used to evaluate polymer properties such as hardness and elastic moduli at the micron scale [47,48]. In the literature, the elastic properties of the investigated materials are often compared by means of the reduced elastic modulus E*, defined as:

$$E^* = \left(\frac{1-\nu_s^2}{E_s} + \frac{1-\nu_i^2}{E_i}\right)^{-1} \quad (4)$$

Where E_s, E_i and ν_s, ν_i are the Young's modulus and the Poisson's ratios of the polymer and the indenter, respectively [49]. With this expression, E* takes into account the polymer-indenter interactions and compensates measurement deviations derived from the indenter deformation and from the indented shape warping. In the present study, the reduced Elastic modulus E* was used to quantify the elastic deformation on all PEEK formulations according to the performed annealing cycle. On the contrary, hardness was not considered here since the inevitable presence of physical imperfections in the indenter tip geometry is a significant problem encountered during hardness evaluation by load–displacement based indentation [50,51]. These geometric tip defects may be comparable to the full indent size and thus cause a significant error in the computed property values [49]. Moreover, considering that the elastic properties of a composite material are known to be particularly meaningful for the determination of the mechanical properties of the composite, according to the macro-mechanical model principles present in the literature, only E* evaluation was performed [52].

3. Results and discussion

3.1 Crystallinity of the annealed samples

The DSC thermograms of the as-molded and annealed samples are illustrated in Figure 2. All thermograms of the as-molded samples showed a single melting endotherm. A previous study [53] demonstrated that the non-isothermal crystallization of the same materials leads to the development of a complex morphology, resulting from the combination of primary, fast and secondary, slow crystallization processes. This behavior is strongly dependent on the time allowed for crystallization and thus on the cooling rate. At high cooling rates (≥50°C/min) the extent of the secondary crystallization was negligible and only the primary crystallization occurred, resulting in a single crystal population, which melted in one simple endotherm in the following DSC scan. Given the molding procedure, the as-molded sample were indeed non-isothermally crystallized at a high cooling rate and showed the expected behavior. The absence of any significant deflection of the baseline below the primary melting endotherm suggested that no significant melting-recrystallization occurred during heating.

All the annealed samples exhibited a secondary melting peak, whose position and intensity varied with the annealing temperature, as already observed in previous studies [38,54]. Table I reports the peak temperatures of both the endotherms observed. The secondary peak was approximately 20-30°C above the annealing temperature, indicating the presence of a population of small, imperfect crystals formed during annealing. The secondary peak shifted towards the primary endotherm as the annealing temperature increased, indicating the formation of thicker crystals for higher treatment temperatures.

While the area of the primary melting peak remained constant independent of the annealing treatment, that of the secondary endotherm increased, as the annealing temperature increased. As a result, the overall crystallinity, calculated according to equation (1), was found to increase between the as-molded and the 300°C annealed material: from 31.9±0.4 to 40.5±0.6%, from 31.5±0.1 to 39.6±0.3% and from 32.3±0.1 to 42.1±0.5% for U, M, and O, respectively (Table II).

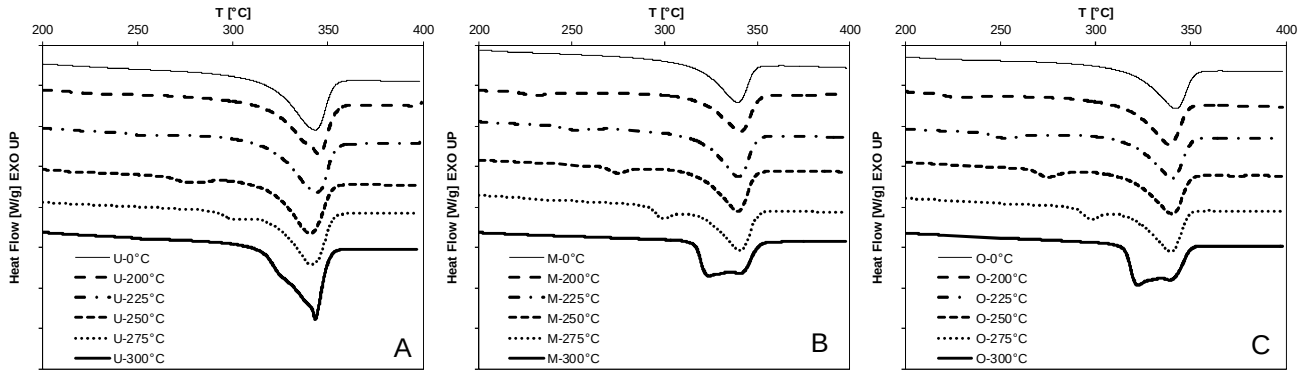

Figure 2. DSC thermograms of samples U (A), M (B) and O (C).

Material (injection moulded samples)	Annealing T [°C]	Tm1 [°C]	Tm2 [°C]
O	-	340.4	
	200	339.2	226.1
	225	339.5	250.3
	250	339.8	275.3
	275	339.3	297.5
	300	339.2	321.2
M	-	340.2	
	200	340.8	228.7
	225	340.1	252.4
	250	340.4	276.6
	275	340.7	299.8
	300	340.9	323.7
U	-	343.3	
	200	345.2	228.8
	225	343.7	251.3
	250	340.7	275.8
	275	341.2	300.1
	300	343.3	324.3

Table I. Melting peak temperatures as a function of the annealing thermal treatment for O, M and U.

In order to check the validity of our assumptions and to confirm the observed trend, FTIR (reflectance mode), WAXD and SAXS measurements were also performed.

FTIR band ratio varied among the annealed samples, ranging from 1.17±0.01 to 1.50±0.04, and constantly increased with the annealing temperature. Table II reports the calculated DSC crystallinity, together with the FTIR band ratio for each material tested.

Material (injection moulded samples)	Annealing T [°C]	DSC crystallinity [%]	FTIR band ratio [1280/1305 cm^{-1}]
U	-	31.9±0.4	1.17±0.01
	200°C	32.8±0.1	1.25±0.01
	225°C	33.9±0.1	1.29±0.01
	250°C	35.3±0.4	1.33±0.01
	275°C	38.5±0.2	1.42±0.03
	300°C	40.5±0.6	1.49±0.01
M	-	31.5±0.1	1.17±0.02
	200°C	31.9±0.3	1.20±0.01
	225°C	33.8±0.1	1.25±0.01
	250°C	34.9±0.1	1.27±0.01
	275°C	38.0±0.5	1.36±0.02
	300°C	39.6±0.3	1.50±0.04
O	-	32.3±0.1	1.17±0.01
	200°C	33.7±0.7	1.19±0.02
	225°C	35.4±0.4	1.18±0.04
	250°C	36.7±0.5	1.23±0.03
	275°C	39.2±0.4	1.31±0.01
	300°C	42.1±0.5	1.44±0.04

Table II. DSC crystallinity %, and FTIR band ratio measurements for U, M and O

Additionally, DSC and FTIR measurements were compared in order to evaluate the correlation between the two methodologies (Figure 3).

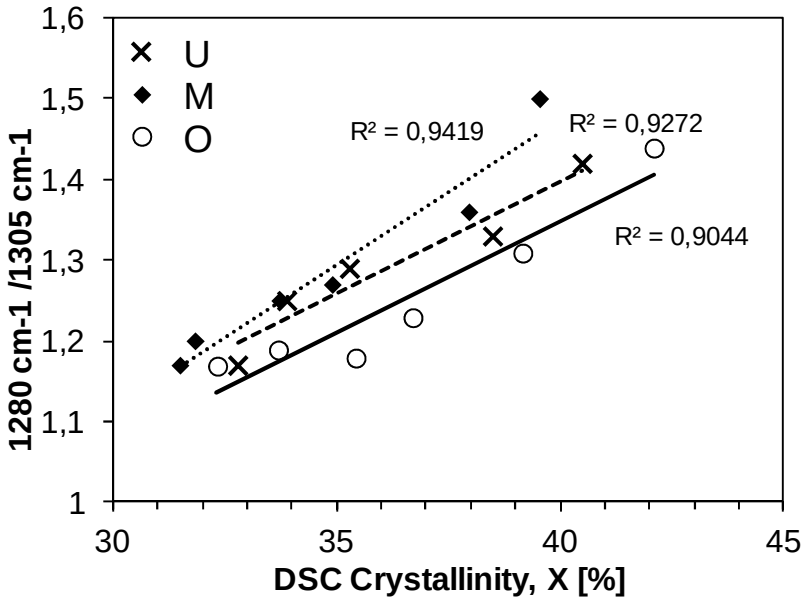

Figure 3. Correlation between DSC and IR measurements.

1280/1305cm^{-1} band ratio and DSC crystallinity percentages showed a favorable correspondence, with a statistical error within 0.9 ($p<0.001$), despite the fact that there was no direct correspondence between the DSC calculated percentage crystallinity and FTIR band ratio among different materials. This can be attributed to the analysis methodology and to samples characteristics: FTIR implies essentially the analysis of superficial material only, while DSC analyzes primarily the bulk material. The two different regions (surface and bulk) might have undergone different cooling gradients following both injection molding process and annealing treatment, and to different extents, leading to the evident discrepancies. In addition, the presence of the carbon fiber can induce small differences in the response to FTIR. This said, data correlation with DSC peak integration was relatively consistent.

In order to provide complementary information on the crystallinity of the tested materials, WAXD measurements were performed. Crystallinity calculation was performed by dividing diffraction peak areas by the amorphous halo area. Diffraction peaks were visible at 2θ approximately equal to 19°, 21°, 23°, 29°, 33°, and 39°, associated with the 110, 111, 200, and 211 planes, respectively whereas the 33° and 39° peaks are not associated with a specific plane orientation [8] and were ignored.

Figure 4 reports the collected WAXD spectra for each material considered. As can be observed, the total counts were lower for the CFR PEEK samples. This could be caused by the difference in density between PEEK and Carbon fibers [41], which caused more absorbance within the reinforced PEEK samples. Also differences in sample thickness could have had an impact on the lower signal intensity observed.

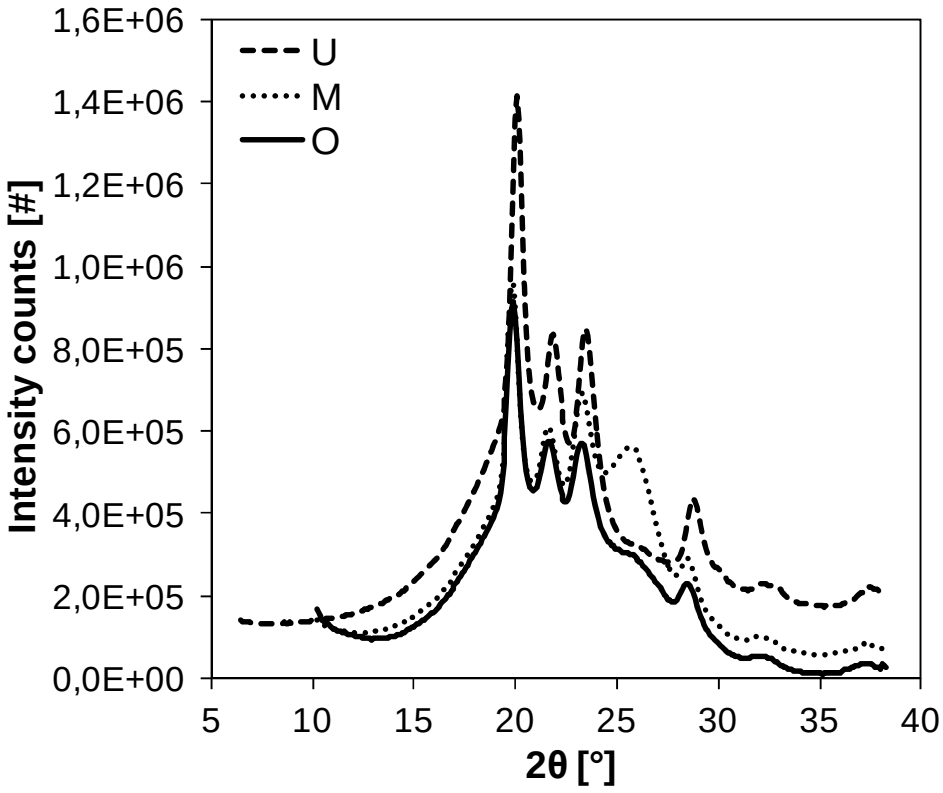

Figure 4. WAXD plots for the untreated samples of U, M and O. CFR formulations have an additional weak signal resulting from the scattering of the carbon fibers at approximately 2θ values of 24°, which is more pronounced for M in respect to O

Data analysis on the calculated crystallinity percentage from WAXD data is reported in Figure 5. As already anticipated by DSC and FTIR measurements, the overall crystallinity progressively increased, as the annealing temperature increased. WAXD data indicated an increase from 28.2 to 34.3%, from 24.1 to 28.8%, and from 28.3 to 37.5% for U, M and O, respectively.

These trends are consistent with the previous findings, indicating that DSC, FTIR, and X-ray diffraction techniques are consistent, despite the fact that the absolute crystallinity percentage was lower than that indicated by DSC measurements.

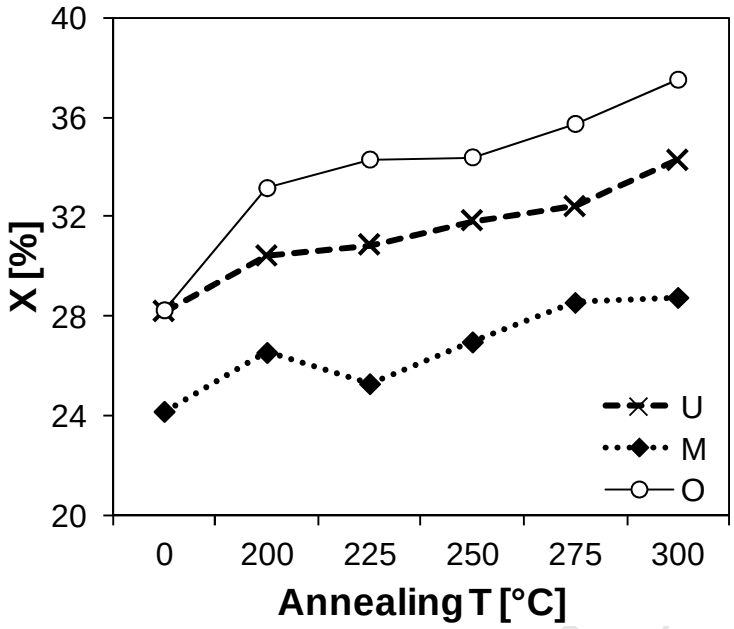

Figure 5. Calculated crystallinity from WAXD diffraction patterns for U, M and O.

Differences in crystallinity between DSC and WAXD measurements are usually explained considering that the area of crystalline reflections, which is summed to provide the crystalline component and then divided by the total background given both by the amorphous halo and the amorphous peak, can be highly increased by the presence of defects/microstrain. As a result, crystallinity associated with WAXD is usually much higher than DSC. In this case however, the carbon fiber peak might have broadened the amorphous peak, resulting in a lowered calculated crystallinity, and in the observed differences among DSC and WAXD results.

WAXD profiles were also used to determine the crystal structure change after the annealing and subsequent cooling treatments by evaluating potential changes in the unit cell parameters. These parameters were calculated using the angular positions of different reflections as

$$a = \frac{\lambda}{\sin\theta_{200}} \tag{5}$$

$$b = \left[\frac{4\sin^2\theta_{110}}{\lambda^2} - \frac{1}{a^2}\right]^{-1/2} \tag{6}$$

$$c = \left[\frac{4\sin^2\theta_{111}}{\lambda^2} - \frac{1}{a^2} - \frac{1}{b^2}\right]^{-1/2} \tag{7}$$

Where λ=0.154 nm is the X-rays wavelength, and θ_{hkl} represents the angular position of the hkl reflection [55].

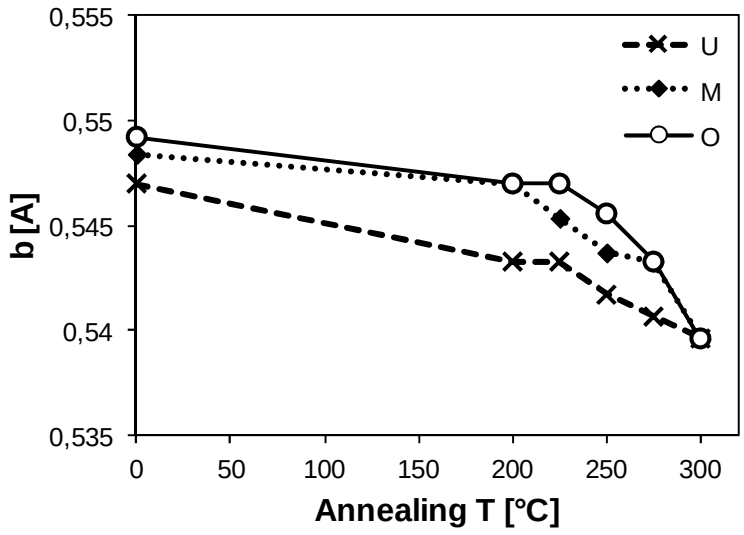

Figure 6. Variations of the unit cell parameter b for U, M and O.

A slight decrease in all the unit cell parameters, most significant for b (Figure 6), was observed for the annealed samples, as already reported in previous studies [56,57]. This indicates that the unit cell density increases with the annealing temperature. Consequently, a higher corresponding crystal density is expected, indicating a closer packing of the lamellae or a greater crystal perfection induced by the thermal treatment.

3.2 Lamellar morphology and dimensions

Further information on lamellar morphology was obtained by performing Small Angle X-ray Scattering (SAXS) measurements on the same specimens used for WAXD analysis. SAXS was used to highlight any potential lamellar thickening occurring upon annealing treatments. The most probable value of interlamellar spacing L (nm) can be calculated from the acquired scattering data according to Bragg's law

$$L = \frac{2\pi}{q} \tag{8}$$

where q is the scattering vector, by individuating the maximum in the first peak of the Lorentz corrected $I \cdot q^2$ vs q plot, which takes into account the theoretical correction that lamellae are infinitely large in two directions [58]. Figure 7 shows the obtained $I \cdot q^2$ versus q plots for all the material formulations herein considered. The plots show that all samples exhibit a broad peak at a decreasing scattering angle q, as the annealing temperature increases. For the CFR-PEEKs, the scattering curves did not decay at high q values, probably due to interference from the fibers or due

to morphology associated with transcrystallinity surrounding the fibers, although no evidences of such have been observed in all the other performed analyses, (attributable to the different sensitivity of the applied techniques). This hypothesis is corroborated by considering that the observed scattering upturn, which is absent in the unfilled U samples and occurs at q values of approximately 1-1.5, must be derived from scatters in the length scale of 4 to 6nm. In the absence of other additives, we must conclude that this scattering may be associated with the presence of small crystallites, which are absent in the unfilled samples and may be associated to transcrystallinity.

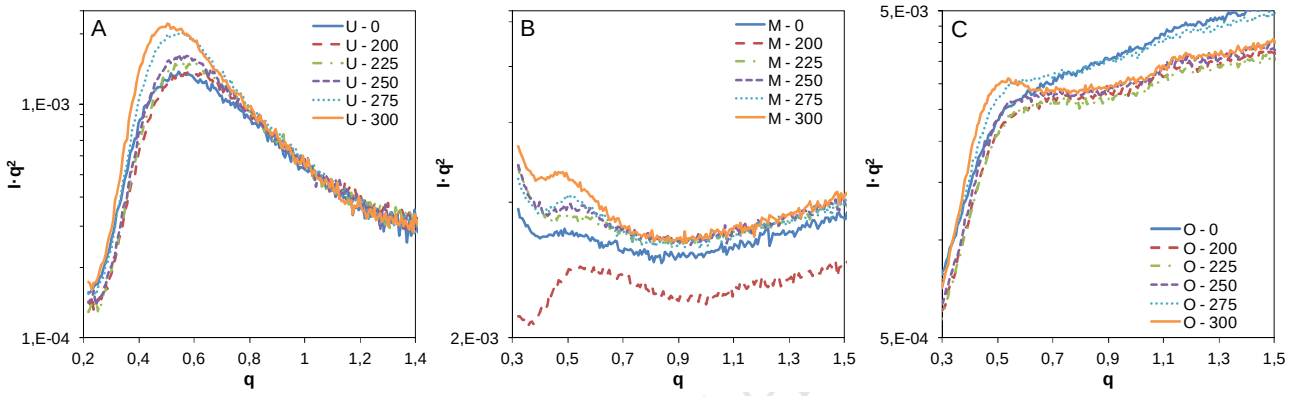

Figure 7.I·q^2 versus q plots for U (A), M (B) and O (C) materials, respectively, for all the annealing temperatures herein considered.

One-dimensional correlation function analysis performed for broader peaks and/or weaker signals variations, is applied by inverse Fourier Transformation of the I·q^2 versus q plots, in order to obtain more precise long period spacing data than by the use of Bragg's law, which was possible for the unfilled PEEK [57].

$$P(x) = \frac{1}{(2\pi^2 A)} \int_0^\infty q^2 I(q) \cos(qr)\, dq \qquad (9)$$

Where P(x) is the paired distance distribution function and, for the case of lamellae, is identical to the one-dimensional correlation function, A is the area of the lamella, I(q) is the experimental scattering function, q is the scattering vector, r is the radial distance perpendicular to the lamellae surfaces within a stack, λ is the wavelength of X-rays (=1.543 Å for CuKα) and θ is half the scattering angle. P(x) was plotted versus r and the value of the first maximum was taken as the inter-lamellar spacing (L).

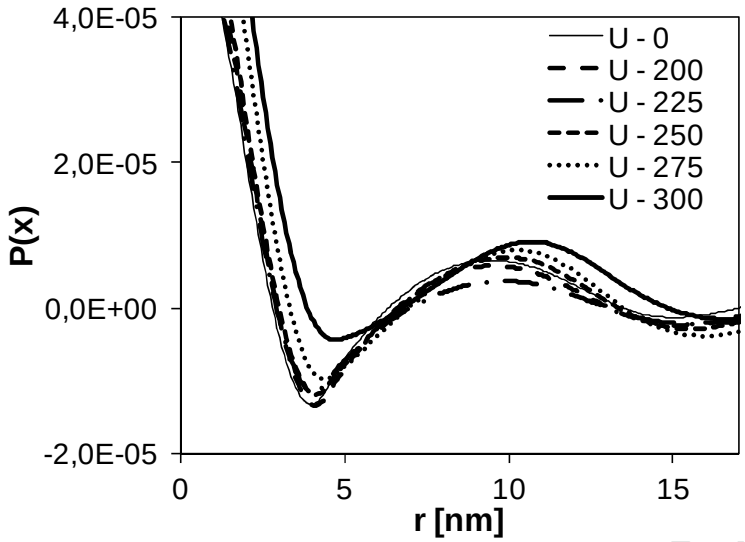

Figure 8. P(x) versus r plot for Ni1 unfilled PEEK.

For the pure polymer, the correlation function well fitted the experimental data (Figure 8). On the contrary, it was not possible to accurately fit the distribution function to both the CFR PEEK scattering profiles, essentially because of two reasons: (i) the significant scattering tail due to the presence of the carbon fiber, and (ii) scattering associated with smaller structures which scatter at high q values (Figure 7). This scattering was outside the angular range of WAXD so it was not expected to be observed in WAXD. As a result, it was not possible to obtain reliable information on the long period for O and M CFR PEEK from the inverse Fourier Transform analysis. The inter-lamellar spacing (L) values for O and M CFR PEEK materials were therefore estimated directly by applying Bragg's law to the $I \cdot q^2$ versus q plots. Lamellar thickness (indicated with s) was calculated by multiplying L by the resulting crystallinity obtained from either WAXD, FT-IR or DSC results. According to previous studies [11], DSC crystallinity was used as a reference. Figure 9 reports the variations in the interlamellar spacing observed, while Table III reports the calculated lamellar thickness values for each of the considered samples.

Annealing T [°C]	**U**		**M**		**O**	
	L [nm]	**s [nm]**	**L [nm]**	**s [nm]**	**L [nm]**	**s [nm]**
0	9.45	3.01	11.12	3.50	8.33	2.69
200	9.52	3.12	11.54	3.68	8.57	2.89
225	9.87	3.35	11.93	4.03	9.00	3.19
250	9.94	3.51	12.33	4.30	9.28	3.41
275	10.29	3.96	12.68	4.82	9.68	3.79
300	10.71	4.34	13.44	5.32	9.86	4.15

Table III. calculated lamellar thicknesses (s) as a function of the annealing temperatures for U, M and O.

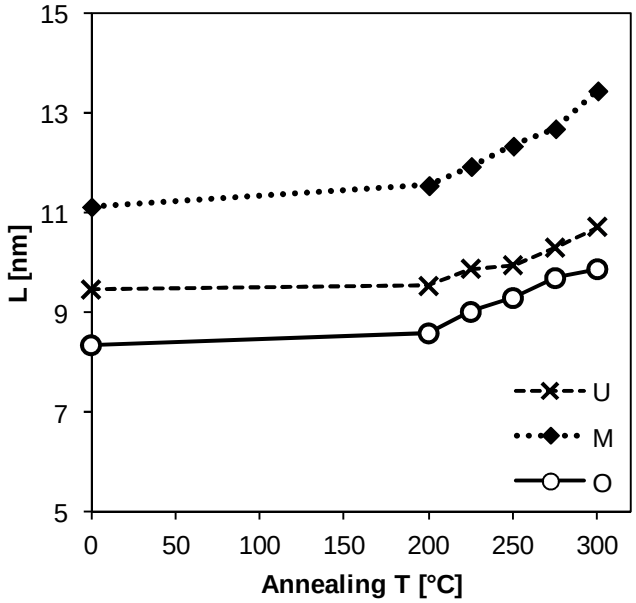

Figure 9. L growth trend according to the annealing treatment temperature for U, M and O

The results indicate that annealing increased the lamellar thickness of all polymer formulations. The lamellar thickness followed the same growth trend observed for the overall crystallinity, indicating that the annealing treatment induce a morphological alteration via lamellar thickening. It must be noted that the lamellar thickening observed using SAXS did not translate into higher peak melting temperature in the DSC experiments. This is likely due to the high sensitivity of SAXS showing less than 3nm increase in thickness of lamellae when comparing control and the highest annealing temperature, which may not show statistically significant changes in the peak melting temperature in DSC. However, SAXS did not show the emergence of a discernible peak at high scattering angles upon annealing demonstrating that scattering was dominated by the original morphology, except that the peak was shifted to a lower scattering angle due to lamellar thickening, which increases long period and thereby decreases the angle of the scattering peak. This is also not entirely surprising since the overall increase in crystallinity comparing control and the PEEK with the highest annealing temperature showed less than 8% difference in crystallinity, and some of this difference in crystallinity can be attributed to lamellar thickening, thereby masking the scattering contributions of the newly formed thin lamellae due to annealing.

3.3 Mechanical properties

Data from the bending test (Figure 10) indicated highly significant differences depending upon the reinforcement type. The mechanical resistance of O composites was much higher than that of M,

since PAN carbon fibers have higher mechanical strength compared to pitch carbon fibers [59], as well as higher flexural modulus, which means higher stiffness of the resulting composite material [41]. Conversely, the resulting bending strength of the U was significantly lower, due to the absence of reinforcements within the polymer.

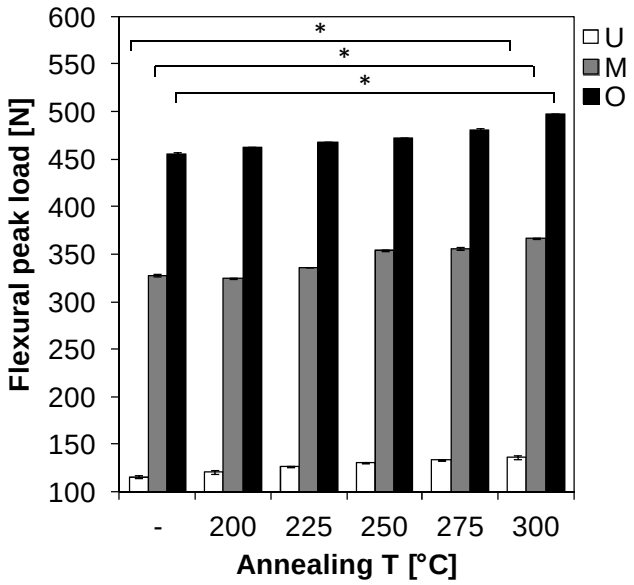

Figure 10. Static bending strength for sample U, M and O.

More interesting though was a significant rise in the mechanical strength with the annealing treatments. Flexural peak load increased by 12% for U (Ni1 unfilled PEEK) and M and by 9% for O samples. In all cases, the variation in the resulting mechanical properties indicates that there is a strong correlation with the resulting crystalline content. Ranging from the untreated material to that annealed at 300°C, the flexural peak load increased by 11% (mean, $p<0.005$), regardless of the material formulation. This result is particularly encouraging for the carbon fiber reinforced materials, since the mechanical properties improvement in a polymer matrix composite material is largely due to the added reinforcement [59].

The same bending strength enhancement trend was observed for unfilled and CFR reinforced formulations, indicating that the failure mechanism in static flexion test was primarily related to the failure of the polymeric matrix. This can be also considered as an indication of a good fiber-matrix interaction in terms of interface adhesion of fibers to the surrounding polymeric matrix.

The nanoindentation test gave further information on the elastic properties of the analyzed materials. Figure 11 reports the reduced Elastic modulus calculation. E* increased with the annealing treatment for all PEEK and CFR PEEK formulations.

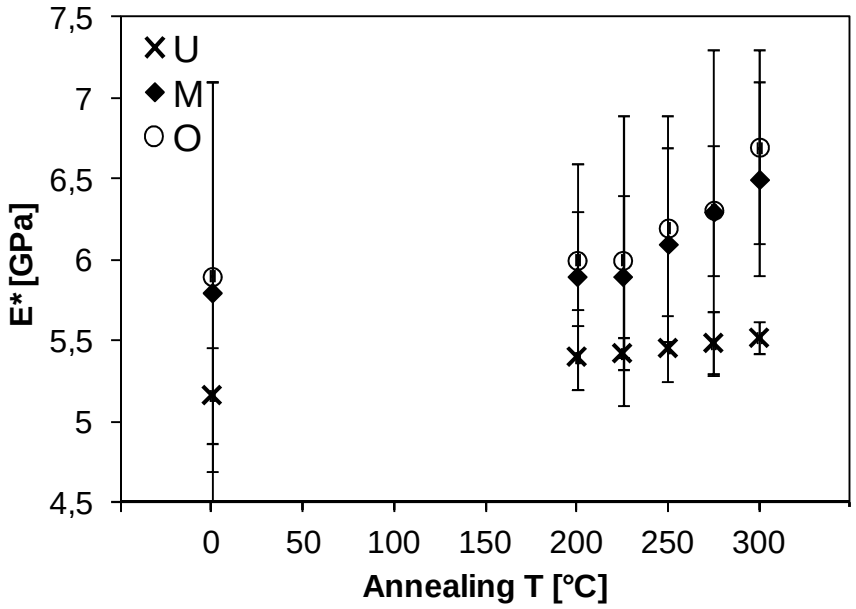

Figure 11. E* modulus for U, M and O at different annealing conditions.

O showed a slight increase in the elastic modulus with increasing annealing temperature: values ranged from 5.9±1.2 to 6.7±0.6GPa for the as molded specimen to the 300°C annealed CFR PEEK, respectively. A similar result was observed for M, whose E* varied from 5.8±1.3 to 6.5±0.6GPa for the as molded specimen and the 300°C annealed one. As already observed for flexural strength, U showed lower properties when compared to M and O CFR formulations: E* varied from 5.2±0.3 to 5.5±0.1GPa for the untreated (as molded) and for the 300°C annealed samples, respectively. The rise in the calculated elastic modulus was linear ($p<0.001$), in contrast to the observation for both CFR PEEK formulations. Data scatter in CFR PEEK samples however was too high to provide statistical significance in those measurements. On the contrary, U showed limited scatter in the data, indicating that the source of scatter in the filled PEEKs was likely the variability in fiber content, interfacial adhesion or the difficulty in avoidance of subsurface fibers during indentation. This is reinforced by the fact that the variability in respective crystallinities was relatively low. In some studies, differences in macroscopic properties between the unreinforced polymer and the reinforced material had been explained by transcrystallization occurring at the fiber matrix interface, which has been proposed to be responsible for enhanced crystallization [60], but this does not seem to be the case here, given the limited differences in crystallinity. In this context, material hardness might have been influenced by the annealing treatments to a greater extent in the fiber-matrix interface region than within the bulk polymer. However, no significant difference was observed in the two CFR samples tested by comparing the calculated E* in the bulk region with the E* obtained from

the fiber-matrix interface investigated areas, probably also due to the increase in data scatter depending on the proximity of subsurface fibers to the indentation and on the indenter penetration area, despite having made indentation measurements in areas where visible fibers were oriented perpendicular to the polished surface, as indicated in Figure 12. Nevertheless, these indentation tests showed a significant increase in the reduced Elastic modulus for unfilled and filled PEEKs, demonstrating modulus reinforcement due to the presence of carbon fibers.

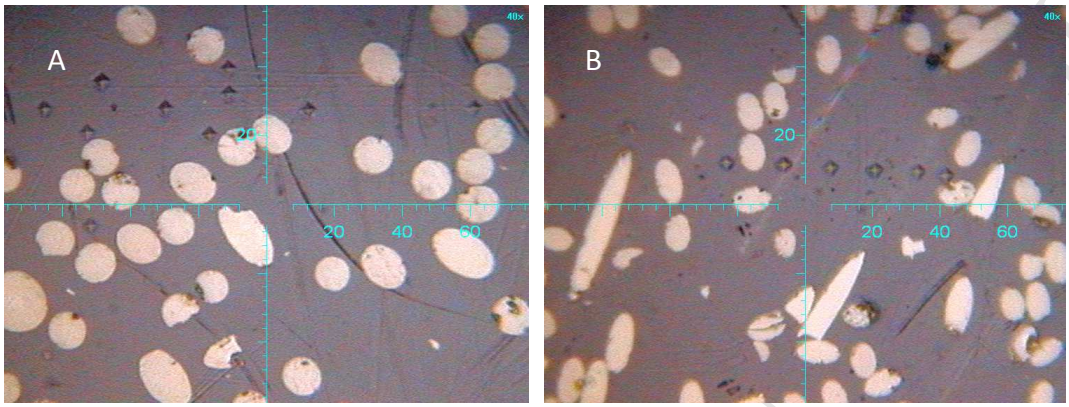

Figure 12. A), M indentations; B), O indentations. An underlying fiber can be clearly discerned at the center of O analyzed section.

4. Conclusion

This study demonstrated that the crystallinity and mechanical properties of PEEK and CFR PEEK varied significantly with the thermal history of the polymer. FTIR, WAXD and SAXS measurements showed an increase in crystallinity by lamellar thickening with annealing temperature. In addition, all the annealed samples exhibited a secondary melting peak in the DSC thermograms, whose position and intensity varied with the annealing temperature, indicating the growth of a population of thinner crystals upon annealing.

Annealing was found to have an impact on PEEK and CFR PEEK mechanical properties, indicating that increase in crystallinity had a strengthening effect in the presence of fiber reinforcement. Further studies are needed to evaluate not only the static, but also the dynamic properties of PEEK, so as to obtain more information on its crystal structure and stability over time and/or in working conditions, as well as on the role of the more complex system associated with fiber-matrix interaction, which is essential to guide in the development of CFR-PEEK composites of high strength and toughness.

References.

[1] M. Biron, Thermoplastics and thermoplastic composites 2nd ed., Plast. Des. Libr. (2013).

[2] S.M. Kurtz, J.N. Devine, PEEK biomaterials in trauma, orthopedic, and spinal implants, Biomaterials. 28 (2007) 4845–4869. doi:10.1016/j.biomaterials.2007.07.013.

[3] Y. Lee, R.S. Porter, Crystallization of poly(etheretherketone) (PEEK) in carbon fiber composites, Polym. Eng. Sci. 26 (1986) 633–639.

[4] Y. Lee, R.S. Porter, Effects of thermal history on crystallization of poly(ether ether ketone) (PEEK), Macromolecules. 21 (1988) 2770–2776.

[5] D.J. Blundell, B.N. Osborn, The morphology of poly(aryl-ether-ether-ketone), Polymer (Guildf). 24 (1983) 953–958. doi:10.1016/0032-3861(83)90144-1.

[6] S.C. Chao, M. Chen, C.T. Chung, Isothermal crystallization and melting behavior of short carbon fiber reinforced poly(ether ether ketone) composites, J. Polym. Res. 5 (1998) 221–226.

[7] M.C. Kuo, J.C. Huang, M. Chen, Non-isothermal crystallization kinetic behavior of alumina nanoparticle filled poly(ether ether ketone), Mater. Chem. Phys. 99 (2006) 258–268. doi:10.1016/j.matchemphys.2005.10.021.

[8] M. Reitman, D. Jaekel, R. Siskey, Chapter 4 – Morphology and Crystalline Architecture of Polyaryletherketones, in: PEEK Biomater. Handb., 2012: pp. 49–60. doi:10.1016/B978-1-4377-4463-7.10004-1.

[9] S. Kumar, D.P. Anderson, W.W. Adams, Crystallization and morphology of poly(aryl-ether-ether-ketone), Polymer (Guildf). 27 (1986) 329–336. doi:10.1016/0032-3861(86)90145-X.

[10] K.N. Krüger, H.G. Zachmann, Investigation of the melting behavior of poly(aryl ether ketones) by simultaneous measurements of SAXS and WAXS employing synchrotron radiation, Macromolecules. 26 (1993) 5202–5208.

[11] C. Fougnies, P. Damman, M. Dosière, M.H.J. Koch, Time-resolved SAXS, WAXS, and DSC study of melting of poly(aryl ether ether ketone) (PEEK) annealed from the amorphous state, Macromolecules. 30 (1997) 1392–1399.

[12] M. Dosière, C. Fougnies, M.H.J. Koch, J. Roovers, Lamellar morphology of narrow PEEK fractions crystallized from the glassy state and from the melt, ACS Symp. Ser. 739 (1999) 166–186.

[13] P. Cebe, S.D. Hong, Crystallization behaviour of poly(ether-ether-ketone), Polymer (Guildf). 27 (1986) 1183–1192. doi:10.1016/0032-3861(86)90006-6.

[14] C.-M. Hsiung, M. Cakmak, J.L. White, Crystallization phenomena in the injection molding of poly ether ether ketone and its influence on mechanical properties, Polym. Eng. Sci. 30

(1990) 967–980. doi:10.1002/pen.760301606.

[15] J.R. Sarasua, P.M. Remiro, J. Pouyet, Effects of thermal history on mechanical behavior of PEEK and its short-fiber composites, Polym. Compos. 17 (1996) 468–477. doi:10.1002/pc.10635.

[16] Y.H. Lai, M.C. Kuo, J.C. Huang, M. Chen, On the PEEK composites reinforced by surface-modified nano-silica, Mater. Sci. Eng. A. 458 (2007) 158–169. doi:10.1016/j.msea.2007.01.085.

[17] S.L. Gao, J.K. Kim, Cooling rate influences in carbon fibre/PEEK composites. Part 1. Crystallinity and interface adhesion, Compos. Part A Appl. Sci. Manuf. 31 (2000) 517–530. doi:10.1016/s1359-835x(00)00009-9.

[18] A. Jonas, R. Legras, J.-P. Issi, Differential scanning calorimetry and infra-red crystallinity determinations of poly(aryl ether ether ketone), Polymer (Guildf). 32 (1991) 3364–3370. doi:http://dx.doi.org/10.1016/0032-3861(91)90540-Y.

[19] G.M.K. Ostberg, J.C. Seferis, Annealing effects on the crystallinity of polyetheretherketone (PEEK) and its carbon fiber composite, J. Appl. Polym. Sci. 33 (1987) 29–39.

[20] B.B. Sauer, W.G. Kampert, E. Neal Blanchard, S.A. Threefoot, B.S. Hsiao, Temperature modulated DSC studies of melting and recrystallization in polymers exhibiting multiple endotherms, Polymer (Guildf). 41 (2000) 1099–1108. doi:10.1016/S0032-3861(99)00258-X.

[21] Y. Kong, J.N. Hay, Multiple melting behaviour of poly(ethylene terephthalate), Polymer (Guildf). 44 (2003) 623–633. doi:10.1016/S0032-3861(02)00814-5.

[22] P. Srimoaon, N. Dangseeyun, P. Supaphol, Multiple melting behavior in isothermally crystallized poly(trimethylene terephthalate), Eur. Polym. J. 40 (2004) 599–608. doi:10.1016/j.eurpolymj.2003.11.003.

[23] D.C. Bassett, R.H. Olley, I.A.M. Al Raheil, On crystallization phenomena in PEEK, Polymer (Guildf). 29 (1988) 1745–1754. doi:10.1016/0032-3861(88)90386-2.

[24] Y. Lee, R.S. Porter, Double-melting behavior of poly (ether ether ketone), Macromolecules. 20 (1987) 1336–1341. doi:10.1021/ma00172a028.

[25] V. Velikov, H. Marand, Studies of the enthalpy relaxation and the “multiple melting” behavior of semicrystalline poly(arylene ether ether ketone) (PEEK), J. Therm. Anal. 49 (1997) 375–383.

[26] L. Jin, J. Ball, T. Bremner, H.J. Sue, Crystallization behavior and morphological characterization of poly(ether ether ketone), Polym. (United Kingdom). 55 (2014) 5255–5265. doi:10.1016/j.polymer.2014.08.045.

[27] X. Tardif, B. Pignon, N. Boyard, J.W.P. Schmelzer, V. Sobotka, D. Delaunay, et al.,

Experimental study of crystallization of PolyEtherEtherKetone (PEEK) over a large temperature range using a nano-calorimeter, Polym. Test. 36 (2014) 10–19. doi:10.1016/j.polymertesting.2014.03.013.

[28] E. Bessard, O. De Almeida, G. Bernhart, Unified isothermal and non-isothermal modelling of neat PEEK crystallization, J. Therm. Anal. Calorim. 115 (2014) 1669–1678. doi:10.1007/s10973-013-3308-8.

[29] G. Zhang, W.Y. Li, M. Cherigui, C. Zhang, H. Liao, J.M. Bordes, et al., Structures and tribological performances of PEEK (poly-ether-ether-ketone)-based coatings designed for tribological application, Prog. Org. Coatings. 60 (2007) 39–44. doi:10.1016/j.porgcoat.2007.06.004.

[30] P.J. Rae, E.N. Brown, E.B. Orler, The mechanical properties of poly(ether-ether-ketone) (PEEK) with emphasis on the large compressive strain response, Polymer (Guildf). 48 (2007) 598–615. doi:10.1016/j.polymer.2006.11.032.

[31] Z. Zhang, C. Breidt, L. Chang, K. Friedrich, Wear of PEEK composites related to their mechanical performances, Tribol. Int. 37 (2004) 271–277. doi:10.1016/j.triboint.2003.09.005.

[32] S.C. Scholes, A. Unsworth, Wear studies on the likely performance of CFR-PEEK/CoCrMo for use as artificial joint bearing materials, J. Mater. Sci. Mater. Med. 20 (2009) 163–170.

[33] N.G. Karsli, S. Demirkol, T. Yilmaz, Thermal aging and reinforcement type effects on the tribological, thermal, thermomechanical, physical and morphological properties of poly(ether ether ketone) composites, Compos. Part B Eng. 88 (2016) 253–263. doi:10.1016/j.compositesb.2015.11.013.

[34] P. Patel, T.R. Hull, R.E. Lyon, S.I. Stoliarov, R.N. Walters, S. Crowley, et al., Investigation of the thermal decomposition and flammability of PEEK and its carbon and glass-fibre composites, Polym. Degrad. Stab. 96 (2011) 12–22. doi:10.1016/j.polymdegradstab.2010.11.009.

[35] Y. Yamamoto, M. Hashimoto, Friction and wear of water lubricated PEEK and PPS sliding contacts Part 2. Composites with carbon or glass fibre, Wear. 257 (2004) 181–189. doi:10.1016/j.wear.2003.12.004.

[36] W.T. Lee, J.Y. Koak, Y.J. Lim, S.K. Kim, H.B. Kwon, M.J. Kim, Stress shielding and fatigue limits of poly-ether-ether-ketone dental implants, J. Biomed. Mater. Res. - Part B Appl. Biomater. 100 B (n.d.) 1044–1052.

[37] V.K. Srivastava, D. Kumar, Prediction of Notched Strength of Laminated Fibre Composites under Tensile Loading Conditions, J. Compos. Mater. . 36 (2002) 1121–1133.

doi:10.1177/0021998302036009581.

[38] H. Quan, Z.M. Li, M.B. Yang, R. Huang, On transcrystallinity in semi-crystalline polymer composites, Compos. Sci. Technol. 65 (2005) 999–1021. doi:10.1016/j.compscitech.2004.11.015.

[39] A.K. Mishra, J.M. Schultz, Kinetics of strain-induced crystallization during injection molding of short fiber composites of poly(ether ether ketone), Polym. Compos. 12 (1991) 169–178. doi:10.1002/pc.750120306.

[40] M. Regis, M. Zanetti, M. Pressacco, P. Bracco, Opposite role of different carbon fiber reinforcements on the non-isothermal crystallization behavior of poly(etheretherketone), Mater. Chem. Phys. 179 (2016). doi:10.1016/j.matchemphys.2016.05.034.

[41] M. Regis, S. Fusi, R. Favaloro, P. Bracco, Composite Science and Technology 2020 - Scientific and Technical Challenges, in: 9th Int. Conf. Compos. Sci. Technol., DEStech Publications Inc (USA), Sorrento, Italy, 2013: pp. 44–56.

[42] M. Chen, C.T. Chung, Crystallinity of isothermally and nonisothermally crystallized poly(ether ether ketone) composites, Polym. Compos. 19 (1998) 689–697.

[43] S.C. Scholes, A. Unsworth, Wear studies on the likely performance of CFR-PEEK/CoCrMo for use as artificial joint bearing materials, J. Mater. Sci. Mater. Med. 20 (2009) 163–170.

[44] J.M. Chalmers, N.J. Everall, K. Hewitson, M.A. Chesters, M. Pearson, A. Grady, et al., Fourier transform infrared microscopy: Some advances in techniques for characterisation and structure-property elucidations of industrial material, Analyst. 123 (1998) 579–586. doi:10.1039/a707070e.

[45] ASTM D790-15e2, Standard Test Methods for Flexural Properties of Unreinforced and Reinforced Plastics and Electrical Insulating Materials, (2015).

[46] T. Iqbal, B.J. Briscoe, S. Yasin, P.F. Luckham, Nanoindentation response of poly(ether ether ketone) surfaces-A semicrystalline bimodal behavior, J. Appl. Polym. Sci. 130 (2013) n/a-n/a. doi:10.1002/app.39723.

[47] W.C. Oliver, An improved technique for determining hardness and elastic modulus using load and displacement sensing indentation experiments, J. Mater. Res. 7 (1992) 1564–1583. doi:10.1557/JMR.1992.1564.

[48] B.J. Briscoe, K. Savio Sebastian, The elastoplastic response of poly(methyl methacrylate) to indentation, Proc. R. Soc. A Math. Phys. Eng. Sci. 452 (1996) 439–457.

[49] T. Iqbal, B.J. Briscoe, P.F. Luckham, Surface Plasticization of Poly(ether ether ketone), Eur. Polym. J. 47 (2011) 2244–2258. doi:10.1016/j.eurpolymj.2011.09.022.

[50] R.H. Ion, H.M. Pollock, C. Roques-Carmes, Micron-scale indentation of amorphous and

drawn PET surfaces, J. Mater. Sci. 25 (1990) 1444–1454. doi:10.1007/BF00585463.

[51] B.D. Beake, G.J. Leggett, M.R. Alexander, Characterisation of the mechanical properties of plasma-polymerised coatings by nanoindentation and nanotribology, J. Mater. Sci. 37 (2002) 4919–4927. doi:10.1023/A:1020830717653.

[52] J.C. Halpin, J.L. Kardos, HALPIN-TSAI EQUATIONS: A REVIEW., Polym. Eng. Sci. 16 (1976) 344–352.

[53] M. Regis, M. Zanetti, M. Pressacco, P. Bracco, Opposite role of different carbon fiber reinforcements on the non-isothermal crystallization behavior of poly(etheretherketone), Mater. Chem. Phys. 179 (2016) 223–231. doi:10.1016/j.matchemphys.2016.05.034.

[54] V. Mylläri, T.-P. Ruoko, J. Vuorinen, H. Lemmetyinen, Characterization of thermally aged polyetheretherketone fibres – mechanical, thermal, rheological and chemical property changes, Polym. Degrad. Stab. 120 (2015) 419–426. doi:10.1016/j.polymdegradstab.2015.08.003.

[55] W. Wang, J.M. Schultz, B.S. Hsiao, Time-Resolved Simultaneous SAXS/WAXS Studies of PEEK during Isothermal Crystallization, Melting, and Subsequent Cooling, J. Macromol. Sci. - Phys. 37 (1998) 667–682.

[56] C. Fougnies, M. Dosière, M.H.J. Koch, J. Roovers, Morphological study and melting behavior of narrow Molecular weight fractions of poly(aryl ether ether ketone) (PEEK) annealed from the glassy state, Macromolecules. 31 (1998) 6266–6274.

[57] T.P. Russell, Small-angle scattering, in: G.S. Brown, D.E. Moncton (Eds.), Handb. Synchrotron Radiation. Vol. 3, North Holland, Amsterdam, 1991: pp. 379–470.

[58] O. Glatter, Data evaluation in small-angle scattering: calculation of the radial electron density distribution by means of indirect Fourier transformation, Acta Phys. Austriaca. 47 (1977) 83–102.

[59] B. Harris, Engineering Composite Materials, 2nd ed., Maney Publishing, Leeds, UK, 1999.

[60] J. Karger-Kocsis, R. Walter, K. Friedrich, Annealing effects on the fatigue crack propagation of injection moulded peek and its short-fibre composites, J. Polym. Eng. 8 (1988) 221–256. doi:10.1515/POLYENG.1988.8.3-4.221.